Electronic Supplementary Material (ESI) for Journal of Materials Chemistry A.

Flexible phase change organohydrogel created from Pickering emulsion technology for thermoelectric conversion and temperature sensing

Yingying He[a], Yuan Wei[a]*, Yangyang Qian[a], Chunyu Wang[a], Yijun Liu[a], Zhixin Ye[a], Gang Chen[a,b]*

[a] State Key Laboratory of Pulp and Paper Engineering, South China University of Technology, Guangzhou 510640, China

[b] Guangdong Engineering Technology Research and Development Center of Specialty Paper and Paper-Based Functional Materials, South China University of Technology, Guangzhou 510640, China

*Corresponding author

E-mail: papercg@scut.edu.cn, wyuan_1122@163.com

Materials

Softwood bleached kraft pulp was supplied from NBKP, Dongguan Lee & Man Paper Manufacturing Co., Ltd. (Dongguan, China). Paraffin wax (PW) with a melting point of 58-60 °C was obtained from Shanghai Yiyang Instrument Co., Ltd (Shanghai, China). Titanium aluminum carbide (Ti_3AlC_2) (400 mesh) were purchased from 11 Technology Co., Ltd. (Jilin, China). Acrylamide (AAm), N,N'-methylene-bis-acrylamide (MBAA), 2,2'-zzobis [2-(2-imidazolin-2-yl) propane] dihydrochloride (AIBI), glycerol, Fe_3O_4 nanoparticles aqueous dispersion (10-30 nm, 25% in H_2O), ethanol, sodium chloroacetate, and sodium hydroxide were purchased by Macklin Biochemical Co. (Shanghai, China) and used without modification.

Characterization

Micromorphology

The morphologies of the CNFs, MXene, and Fe_3O_4 were characterized by an Atomic force microscope (AFM, Multimode 8, Bruker, Germany), and the NanoScope Analysis 1.5 software was used to calculate the average height difference between the peaks and the base line according to the AFM images. The micromorphology of the Pickering emulsion droplets was revealed using a confocal laser scanning microscopy (CLSM, Leica TCS-SP5, Germany), where the sample was put on a glass slide with a coverslip to observe. The aqueous phase and oil phase in emulsion gels was dyed by rhodamine B and Nile Red, respectively. The surface morphologies and microstructures of the samples were analyzed by field emission scanning electron microscopy (SEM) with an element mapping apparatus (Merlin, Zeiss, Germany). X-ray diffraction (XRD, D8 ADVANCE, Bruker, Germany) was employed to explore the crystal structure of Ti_3AlC_2 and MXene with the Cu Kα radiation at a range of 2θ=5-80°.

Mechanical properties

The mechanical properties of the organohydrogels were measured by a Instron

3300 universal testing machine (Instron Ltd., America) equipped with a 500 N load cell, under a stretching speed of 40 mm/min at ambient temperature. To ensure accuracy, at least five parallel measurements were carried out for each sample and the average value was calculated. Self-recovery properties were investigated by typical successive loading-unloading tests at 30 % strain, where successive 1 000 cycles were conducted without intervals between consecutive cycles.

Thermal properties

The enthalpy (ΔH_m and ΔH_c), melting temperature (T_m), and crystallization temperature (T_c) of the organohydrogels were measured using a differential scanning calorimetry (DSC, Netzsch DSC 214 Polyma DSC21400A-0318-L, Germany) under a nitrogen atmosphere with a flow rate of 40 mL min^{-1}. These samples were carried out by heating from -150 °C to 80 °C and then cooling from 80 to -150 °C at the heating rate of 10 °C min^{-1}. Heating, cooling, and reheating cycles were performed. For all samples, the temperature was maintained at 80 °C for 5 min to eliminate the thermal history of the first heating cycle. The thermal stability of the samples was investigated via thermal cycle tests. The sample was placed on a heating stage, and heated to 80 °C and then cooled to room temperature by adjusting the heating controller. This process was performed consecutively for 50 times. Moreover, an infrared imaging device (Fluke Ti27, American) was used to record the temperature variation of the samples during heating and cooling processes.

Temperature and hot-steam response characterization

The resistance variations of the organohydrogel sensor in response to different temperatures and hot steams were measured by an electrochemical workstation (CHI 660E, China) under an open circuit voltage of 1 V, which combined with a computer and corresponding data acquisition system. Thus, the real-time resistance variations were recorded when different heat/cool sources approached and took away.

Table S1. Experimental recipes for preparing Pickering emulsions stabilized by CNF-MXene-Fe_3O_4.

Samples	Water : oil (V/V)	Mass ratio of CNF (wt%)	Glycerol (wt%)	Mass ratio of MXene (wt%)	Mass ratio of Fe_3O_4 (wt%)
CMFPG-P**7**	**7:1**	0.5	35	0.9	3.0
CMFPG-P**8**	**8:1**	0.5	35	0.9	3.0
CMFPG-P**9**	**9:1**	0.5	35	0.9	3.0
CMFPG-P**10**	**10:1**	0.5	35	0.9	3.0
$C_{\mathbf{0.4}}$MFPG-P7	7:1	**0.4**	35	0.9	3.0
$C_{\mathbf{0.3}}$MFPG-P7	7:1	**0.3**	35	0.9	3.0
$C_{\mathbf{0.2}}$MFPG-P7	7:1	**0.2**	35	0.9	3.0
$C_{\mathbf{0.1}}$MFPG-P7	7:1	**0.1**	35	0.9	3.0
CMFP-P7	7:1	0.5	**0**	0.9	3.0
$CM_{0.5}$FPG-P7	7:1	0.5	35	**0.5**	3.0
$CM_{0.2}$FPG-P7	7:1	0.5	35	**0.2**	3.0
CM_0FPG-P7	7:1	0.5	35	**0**	3.0
$CMF_{1.5}$PG-P7	7:1	0.5	35	0.9	**1.5**
CMF_0PG-P7	7:1	0.5	35	0.9	**0**

[a] The density of PW is 0.9 g/cm^3.

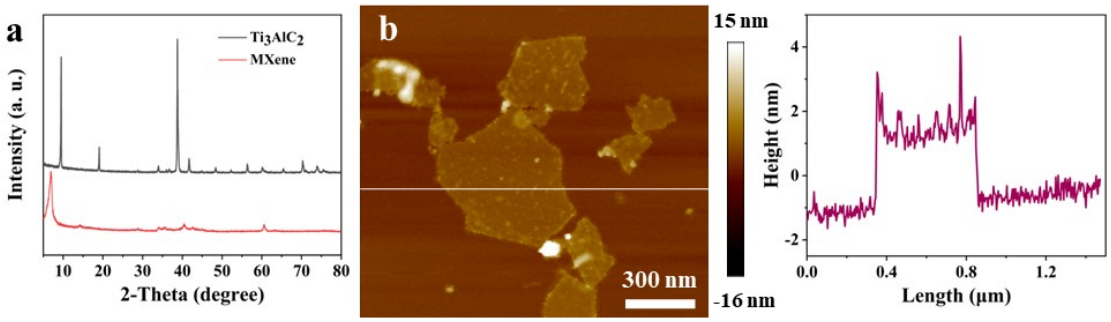

Fig. S1 (a) XRD patterns of Ti_3AlC_2 and MXene nanosheets. (b) AFM image of the MXene (left) and the height profile (right) along the white line in the AFM image.

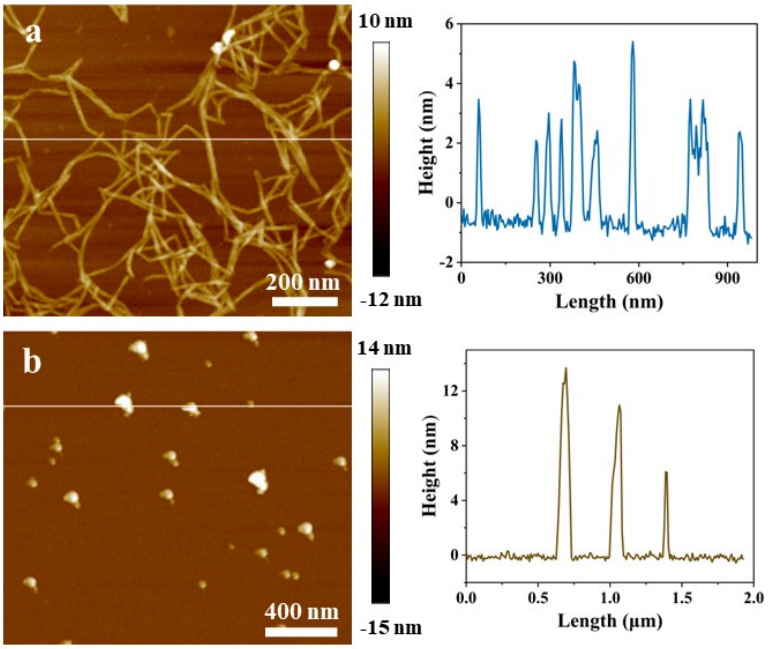

Fig. S2 AFM images of the (a) CNFs (left) and (b) Fe_3O_4 nanoparticles (left), as well as the height profile (right) along the white line in the AFM images.

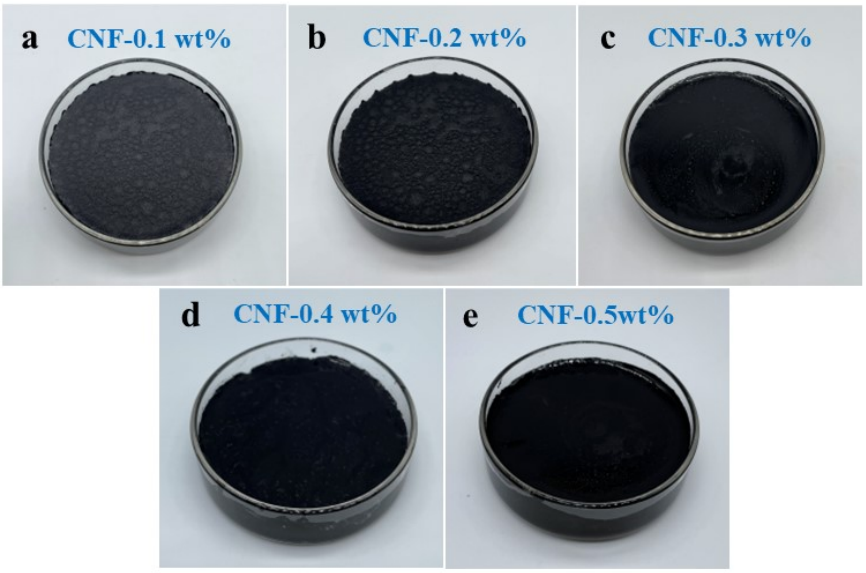

Fig. S3 Digital photos of the CMFAG-P Pickering emulsions with different CNF concentration of (a) 0.1 wt%, (b) 0.2 wt%, (c) 0.3 wt%, (d) 0.4 wt%, and (e) 0.5 wt%.

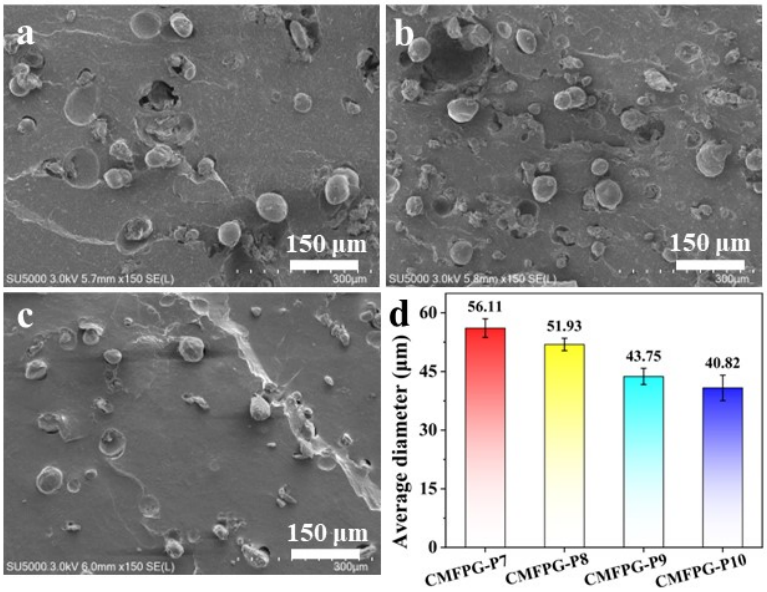

Fig. S4 SEM images of the (a) CMFPG-P8, (b) CMFPG-P9, and (c) CMFPG-P10 organohydrogels. (d) Average diameters of the PW microspheres in CMFPG-P organhydrogels. (The number of paraffin microspheres for the calculation was ≈ 20)

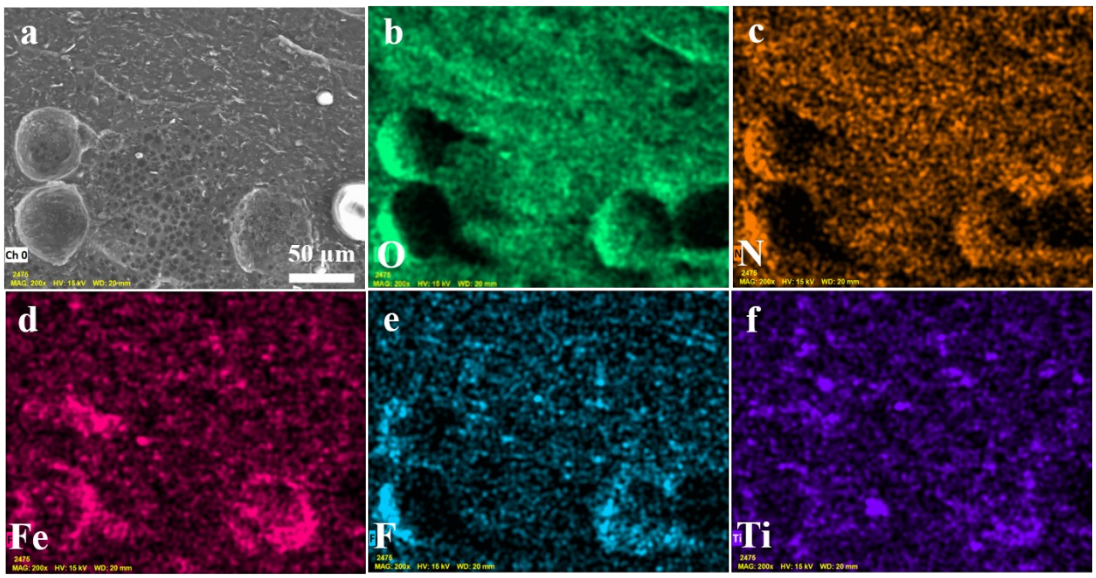

Fig. S5 (a) SEM image of the CMFPG-P7 organohydrogel and (b-f) elemental mapping images of the (b) O, (c) N, (d) Fe, (e) F, and (f) Ti elements in CMFPG-P7 organohydrogel.

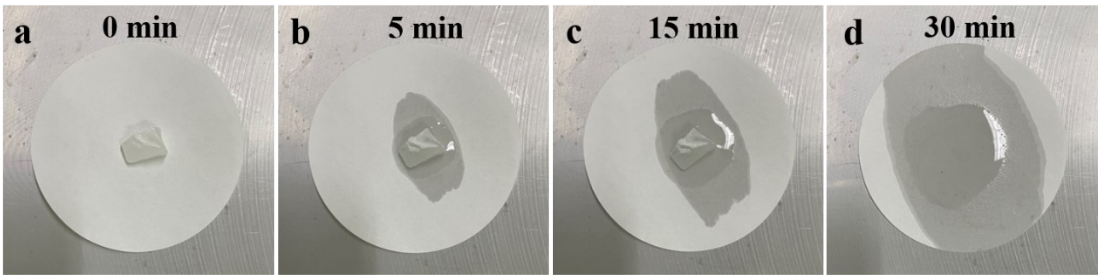

Fig. S6 Digital images of the melting process of the bulk PW.

Table S2. Thermal properties of the pure PW, CMFPG and CMFPG-P organohydrogels.

Samples	T_{m1} (°C)	T_{m2} (°C)	ΔH_m (J/g)	T_{c1} (°C)	T_{c2} (°C)	ΔH_c (J/g)
PW	44.0	62.3	221.27	38.3	51.6	223.32
CMFPG	-	-	-	-	-	-
CMFPG-P7	44.0	60.7	21.12	38.6	54.5	21.32
CMFPG-P7 after 50 thermal cycles	44.2	61.0	16.82	38.2	54.2	17.95
CMFPG-P8	44.1	60.5	17.12	38.7	55.0	13.81
CMFPG-P9	43.9	60.3	14.95	39.1	55.2	13.01
CMFPG-P10	44.7	60.8	13.16	38.5	54.6	12.15

Where T_{m1}, T_{m2}, and ΔH_m represent the melting temperature of solid-solid phase transition, the melting temperature of solid-liquid phase transition, and the melting enthalpy of samples during solid-liquid transition, respectively. T_{c1}, T_{c2}, and ΔH_c represent the crystallization temperature of solid-solid phase transition, the crystallization temperature of liquid-solid transition, and the crystallization enthalpy of samples during solid-liquid transition, respectively.

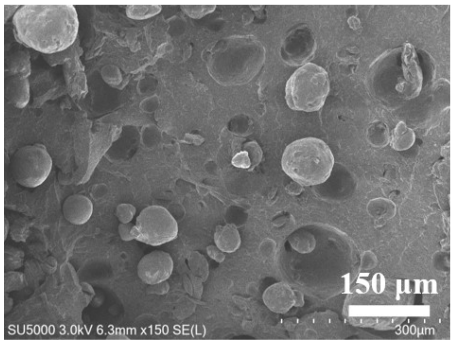

Fig. S7 SEM image of the CMFPG-P7 organohydrogel after 50 thermal cycles.

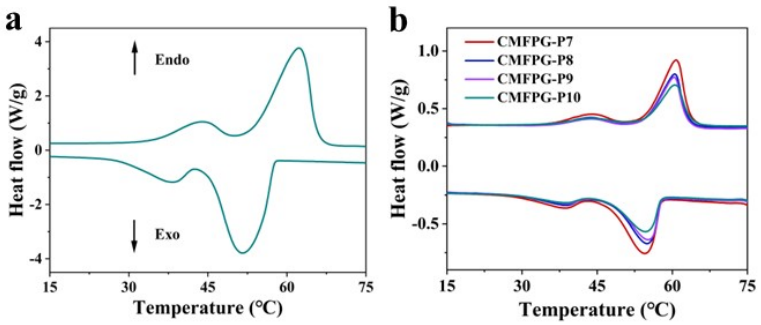

Fig. S8 DSC curves of (a) the PW and (b) CMFPG-P organohydrogels.

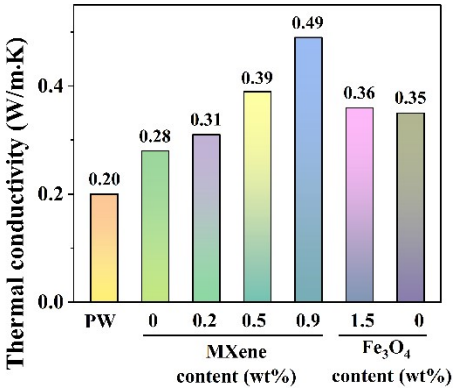

Fig. S9 Thermal conductivity of the PW and CMFPG-P7 organohydrogel with different contents of MXene and Fe_3O_4.

Table S3. Comparison of the thermal conductivity between $C_{0.5}M_{0.9}F_{3.0}$PG-P7 organohydrogel and other PW-based composites.

Samples	Thermal conductivity (W/mK)	References
PW/poly(styrene-b-ethylene-co-butylene-b-styrene)/reduced graphene oxide	0.44	43
PW/Fe_3O_4/polypropylene/carbon nanotubes	0.59	44
PW/SiO_2 carbon nanofiber	0.73	45
PW/multi-walled carbon nanotube	0.33	46
PW/garlic stem biochar	0.31	47
PW/polyethylene/carbon nanotubes	0.43	48
PW/Fe_3O_4	0.33	49
$C_{0.5}M_{0.9}F_{3.0}$PG-P7	0.49	This work

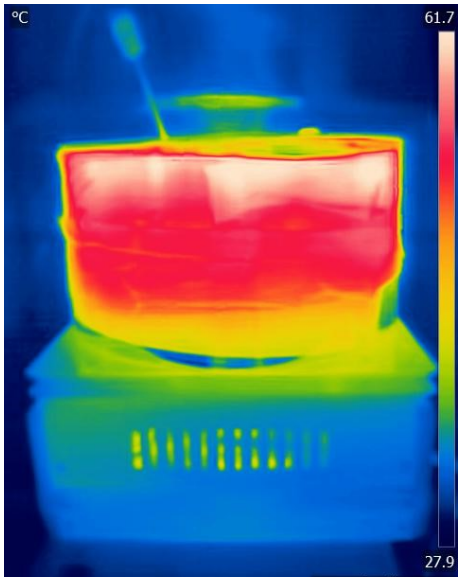

Fig. S10 Thermal infrared image of the water bath device.

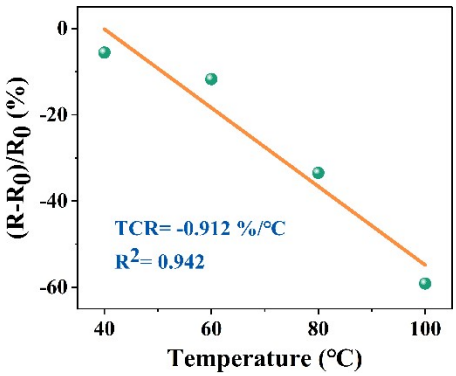

Fig. S11 Relative resistance variation of the CMFPG-P7 organohydrogel-based sensor for hot steam with different temperatures.

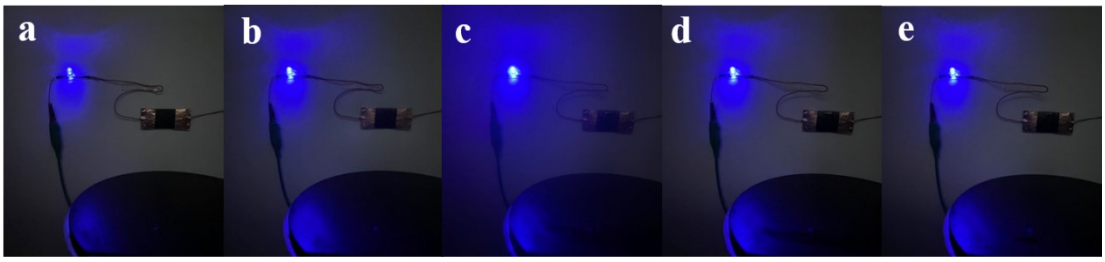

Fig. S12 Digital photos of the brightness of light-emitting diode (LED) light.